ENGINEERING

A wireless and battery-free wound infection sensor based on DNA hydrogel

Ze Xiong[1,2,3]†*, Sippanat Achavananthadith[1]†, Sophie Lian[4]†, Leigh Edward Madden[5,6], Zi Xin Ong[5,6,7], Wisely Chua[8], Viveka Kalidasan[1], Zhipeng Li[1], Zhu Liu[1], Priti Singh[9], Haitao Yang[10], Sascha P. Heussler[11], S. M. P. Kalaiselvi[12], Mark B. H. Breese[12], Haicheng Yao[13], Yuji Gao[2], Kavitha Sanmugam[14], Benjamin C. K. Tee[1,2,3,13,15], Po-Yen Chen[10], Weiqiang Loke[9], Chwee Teck Lim[2,4,15,16], Grace Shu Hui Chiang[14], Boon Yeow Tan[14], Hao Li[7,17], David Laurence Becker[5,6], John S. Ho[1,2,3,15]*

The confluence of wireless technology and biosensors offers the possibility to detect and manage medical conditions outside of clinical settings. Wound infections represent a major clinical challenge in which timely detection is critical for effective interventions, but this is currently hindered by the lack of a monitoring technology that can interface with wounds, detect pathogenic bacteria, and wirelessly transmit data. Here, we report a flexible, wireless, and battery-free sensor that provides smartphone-based detection of wound infection using a bacteria-responsive DNA hydrogel. The engineered DNA hydrogels respond selectively to deoxyribonucleases associated with pathogenic bacteria through tunable dielectric changes, which can be wirelessly detected using near-field communication. In a mouse acute wound model, we demonstrate that the wireless sensor can detect physiologically relevant amounts of *Staphylococcus aureus* even before visible manifestation of infection. These results demonstrate strategies for continuous infection monitoring, which may facilitate improved management of surgical or chronic wounds.

INTRODUCTION

Wearable biosensors linked with smartphones provide an opportunity to detect pathophysiological events in real time to notify patients and their caregivers (*1*–*8*). Such technology has the potential to transform the diagnosis, prevention, and management of chronic medical conditions by enabling continuous monitoring outside of traditional clinical settings. Chronic wounds represent one such condition where management is a major health care challenge, consuming over 5% of the health care budget (*9*). A key factor contributing to the inability of chronic wounds to heal is the presence of pathogenic bacteria, which secrete virulent enzymes that destroy host tissues and disrupt wound recovery (*10*, *11*). Prompt detection of wound infection is thus critical for clinical intervention to improve patient outcomes (*12*). However, current methods for detection rely on either subjective clinical assessments or time-consuming culture-based laboratory tests (*13*, *14*), leading to delays in timely administration of proper treatment.

Recent advances in flexible electronics have yielded a variety of sensing concepts for interfacing with wounds and tracking clinically relevant parameters. The most advanced sensors for this purpose measure parameters with well-established methods of electronic transduction, such as temperature, pressure, humidity, and pH (*15*–*22*). These parameters can afford insights about the local wound environment but do not directly reflect bacterial virulence. Using optical and electrochemical techniques, biosensors capable of detecting specific markers of pathogenic bacteria at the point of care have been developed (*23*–*25*). However, the integration of such sensors into a wearable device is challenging because of the complexity of the readout instrumentation. Stimuli-responsive materials provide an alternative sensing approach where biological signals are transduced into conveniently detectable changes in material properties (*26*, *27*). Because of their broadly tunable, tissue-like mechanical properties (*28*, *29*), stimuli-responsive hydrogels have been widely exploited for sensing applications, such as colorimetric indicators of wound pH (*30*, *31*). Although recent work demonstrates strategies to extend the programmability and response of hydrogels (*32*, *33*), existing sensors still lack the ability to detect wound infection and wirelessly transmit data in a way that enables the wound to be continuously monitored without disturbance.

Here, we propose and demonstrate a sensing technology, termed wireless infection detection on wounds (WINDOW), which detects bacteria virulence using a flexible, wireless, and battery-free sensor. This sensor is based on a custom DNA hydrogel (DNAgel) that provides a radio frequency detectable response to deoxyribonuclease (DNase), an enzyme secreted by opportunistic pathogens—including *Staphylococcus aureus*, *Pseudomonas aeruginosa*, and *Streptococcus pyogenes*—commonly implicated in clinical wound infections but not substantially produced by skin-colonizing commensal bacteria (*34*–*36*). DNase can act as a virulence factor that facilitates bacteria

[1]Department of Electrical and Computer Engineering, National University of Singapore, Singapore 117583, Singapore. [2]Institute for Health Innovation and Technology, National University of Singapore, Singapore 117599, Singapore. [3]The N.1 Institute for Health, National University of Singapore, Singapore 117456, Singapore. [4]Department of Biomedical Engineering, National University of Singapore, Singapore 117583, Singapore. [5]Lee Kong Chian School of Medicine, Nanyang Technological University, Singapore 308232, Singapore. [6]Skin Research Institute of Singapore, Singapore 308232, Singapore. [7]Nanyang Institute of Technology in Health and Medicine, Interdisciplinary Graduate Programme, Nanyang Technological University, Singapore 637335, Singapore. [8]Institute of Molecular and Cell Biology, A*STAR, Singapore 138669, Singapore. [9]Faculty of Dentistry, National University of Singapore, Singapore 119085, Singapore. [10]Department of Chemical and Biomolecular Engineering, National University of Singapore, Singapore 117585, Singapore. [11]Attonics Systems Pte Ltd., Singapore 079903, Singapore. [12]Singapore Synchrotron Light Source, National University of Singapore, Singapore 117603, Singapore. [13]Department of Materials Science and Engineering, National University of Singapore, Singapore 117575, Singapore. [14]St Luke's Hospital, Singapore 659674, Singapore. [15]Graduate School of Integrative Sciences and Engineering, National University of Singapore, Singapore 117456, Singapore. [16]Mechanobiology Institute, National University of Singapore, Singapore 117411, Singapore. [17]Department of Chemistry, National University of Singapore, Singapore 117544, Singapore.
*Corresponding author. Email: elexio@nus.edu.sg (Z.X.); johnho@nus.edu.sg (J.S.H.)
†These authors equally contributed to this work.

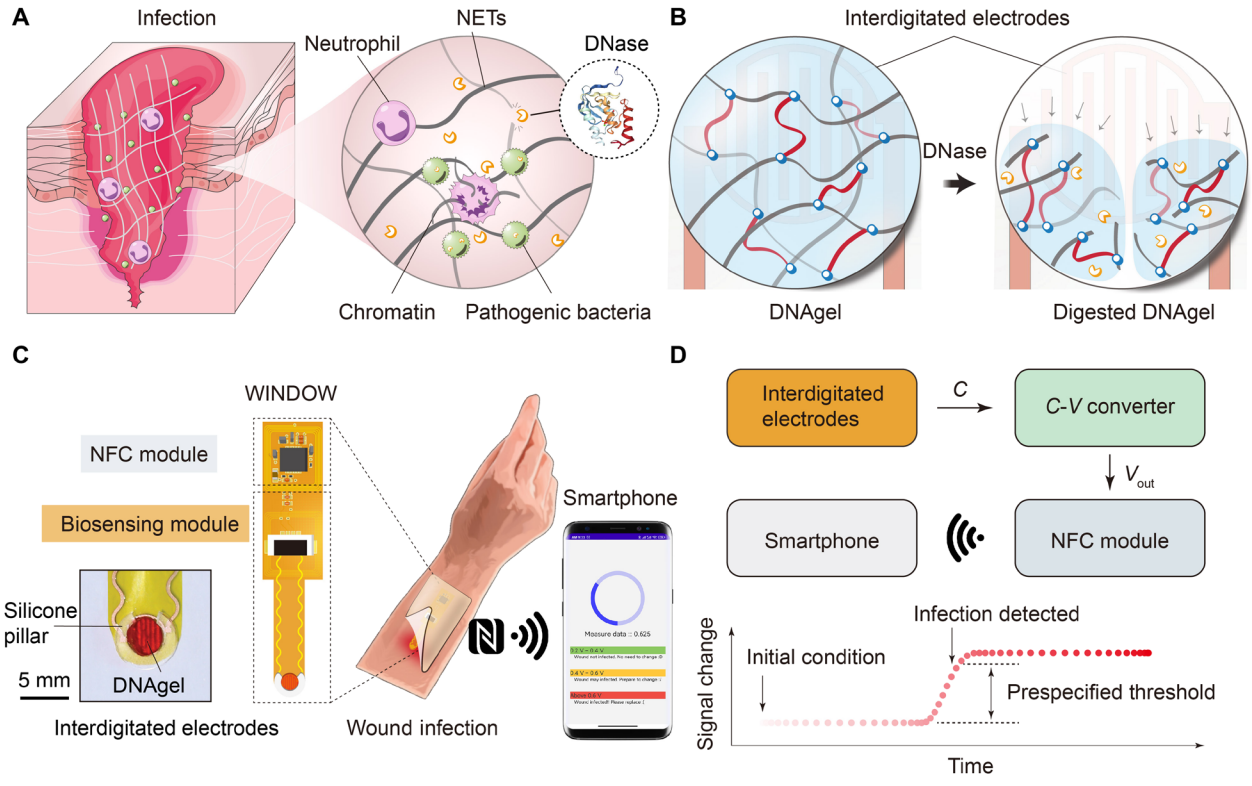

Fig. 1. WINDOW concept. (**A**) DNase is a virulence factor in wound infections. Pathogenic bacteria secrete DNase to evade neutrophil extracellular traps (NETs), which are integral to the host's immune response. (**B**) Schematic of the infection sensing mechanism. DNAgel is degraded upon exposure to DNase, resulting in a change in the capacitance of the sensor. (**C**) Schematic of the wireless wound infection sensor. WINDOW integrates the bioresponsive DNAgel, a half-wave–rectified *LC* biosensing module, and an NFC module to enable smartphone readout of the wound status. Inset image: Sensor-integrated DNAgel stained with rhodamine B. (**D**) System block diagram showing signal transduction from the DNAgel-based biosensor to the NFC module and to a smartphone for wireless readout and display.

dissemination from biofilms and bacteria evasion of neutrophil extracellular traps deployed by the host immune defense (Fig. 1A) (*37*). When exposed to extracellular DNase, the DNAgel is degraded via nonspecific cleavage of DNA strands, resulting in dissolution of the hydrogel. This changes the dielectric permittivity of the region above an interdigitated electrode and therefore modulates its capacitance (Fig. 1B and note S1). By connecting the electrode to an embedded system, this electronic signal can be read out in a wireless and battery-free manner using near-field communication (NFC), a connectivity technology found on most modern smartphones for short-range communication and wireless power transfer (Fig. 1C and note S2) (*4*, *38*, *39*). WINDOW has a thin and flexible form factor that enables it to be conformally embedded into wound dressings to wirelessly track virulence factor activity on demand (Fig. 1D). We demonstrate the potential of WINDOW for real-time detection of clinically relevant amounts of *S. aureus* both in vitro and in a mouse wound model before visible manifestation of infection. This technology may facilitate timely detection of wound infections for improved management of surgical or chronic wounds.

RESULTS

DNAgel synthesis and processability

To convert DNase activity into a smartphone-readable signal, we developed a DNAgel that meets processability requirements for integration into a bioelectronic sensor and exhibits a chemically tunable dielectric permittivity over the radio frequency spectrum. In contrast to previous work that used heating-cooling cycles to form physically crosslinked DNAgel (*40*), we used a chemical crosslinking strategy to provide increased stability in aqueous environments and capacity for functionalization (see Materials and Methods; Fig. 2, A and B; and fig. S1) (*41*). This strategy yields a DNAgel with several advantageous properties: (i) less steric hindrance to subsequent permittivity engineering, (ii) fewer DNA strands (~0.05 g of dehydrated DNA in 1 ml of DNAgel) for increased sensitivity to DNase, and (iii) greater diffusion of reactive agents through the three-dimensional (3D) network for more rapid response time. The gelation reaction can be completed at room temperature without requiring heating or other harsh conditions. The ability of DNAgel to be gelated in situ enables it to be integrated into a wide range of bioelectronic interfaces. For instance, DNAgel precursor can be printed on either planar surface (Fig. 2, C and G) or curved contact lens (Fig. 2, D and H) or be molded into 3D macrostructures (Fig. 2, E and I) and microstructures (Fig. 2, F and J) with a spatial resolution as fine as 10 μm (movie S1).

Selective bioresponse and anti-dehydration capability of DNAgel

The selective degradation of DNAgel by DNases associated with pathogenic bacteria provides the reporting mechanism for detection of an active wound infection. We first validated that DNAgel is selectively degraded by the opportunistic pathogen *S. aureus* ATCC

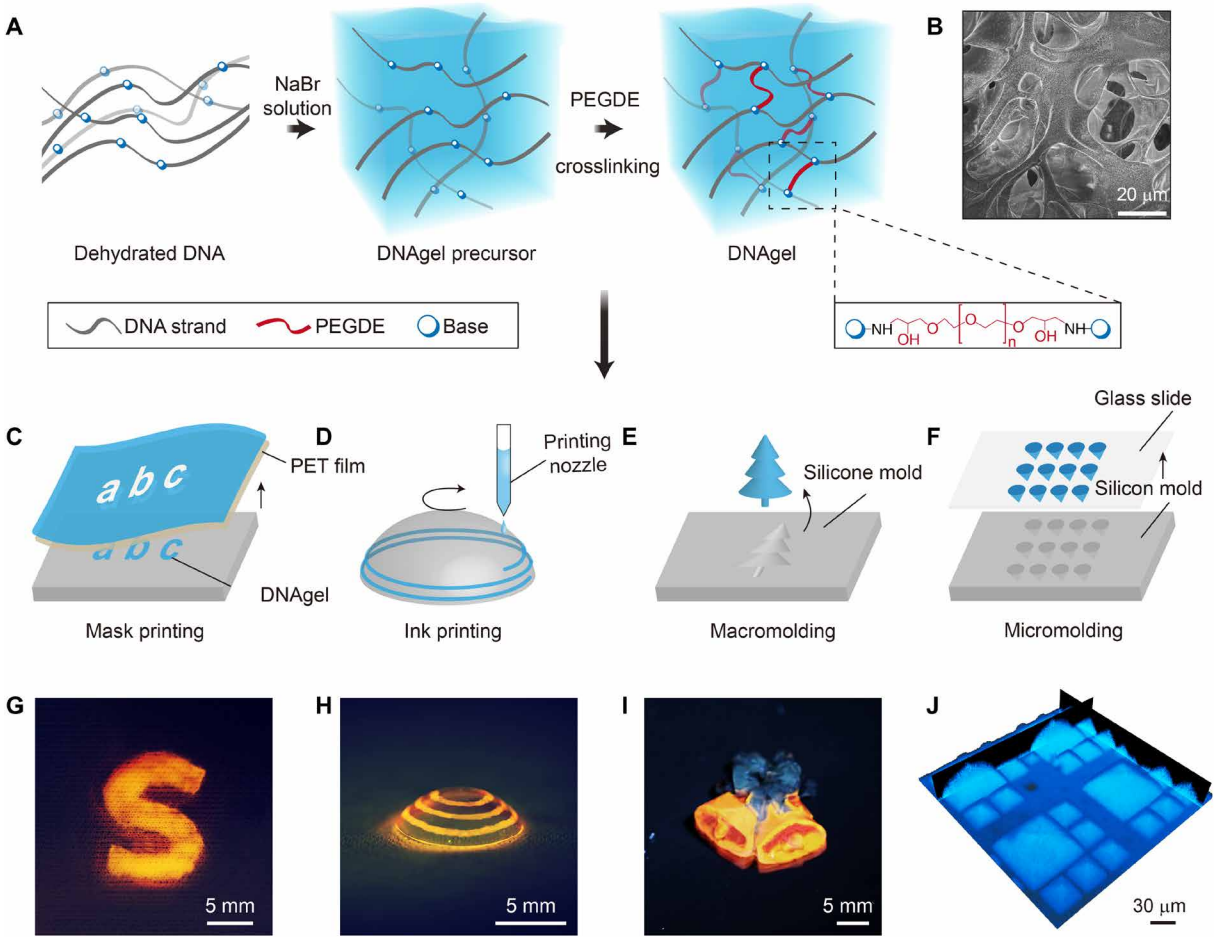

Fig. 2. DNAgel synthesis and processability. (**A**) Schematic of the synthesis process. DNAgel precursor is prepared by dissolving dehydrated DNA strands and then chemically crosslinked by poly(ethylene glycol) diglycidyl ether (PEGDE), forming a 3D network at room temperature. (**B**) Scanning electron microscope image of freeze-dried DNAgel. (**C** to **F**) Strategies for processing DNAgel. DNAgel can be printed on planar (C) and curved surfaces (D) or molded into 3D structures at millimeter (E) to micrometer (F) scales. (**G** to **I**) Images of fluorescence-stained DNAgel formed into the letter S (G), printed on a contact lens (H), and macromolded into a Christmas bell (I). (**J**) 3D confocal fluorescent image of DNAgel pyramids formed by micromolding. The smallest micropyramid is ~10 μm.

(American Type Culture Collection) 29213. DNAgel droplets were coincubated with live neonatal human dermal fibroblasts (NHDFs) or *S. aureus* culture with comparable total cellular volume (fig. S2). Confocal fluorescence imaging showed that coincubation with NHDFs (~2×10^4 cells) for over 1 hour resulted in negligible change in the droplet morphology (Fig. 3A). In contrast, coincubation with *S. aureus* culture [~7×10^7 colony-forming units (CFU)] for 1 hour resulted in complete degradation of the DNAgel droplet (Fig. 3B and movie S2). DNAgel degradation can be attributed to secretion of DNase (nuclease S7, also known as micrococcal nuclease) by *S. aureus*, as shown by immersing DNAgel (~2.3×10^8 μm^3 in volume) into a DNase solution (~1 U/μl) (Fig. 3C and fig. S3). 3D topography reconstructions show that DNAgel volume is reduced by 56% after 1 hour of immersion (Fig. 3, D and E) and 68.3% after 1.5 hours (movie S3). We further assessed the selective degradation of DNAgel by *S. aureus* compared to a panel of commensal skin-associated bacteria by incubating DNAgel with the respective sterile-filtered bacteria culture supernatant. Whereas DNAgel incubated with *S. aureus* over 24 hours exhibited about 70% decrease in fluorescence intensity, DNAgel incubated with other skin commensal bacteria prevalent on the epidermis were not substantially degraded (fig. S4).

We further evaluated the ability of the DNAgel to detect *S. aureus* infection in wound swabs collected from diabetic foot ulcer (DFU) patients. From a cohort of 18 DFU patients with available clinical microbiology reports, 3 patients were positive for *S. aureus*. We determined the total CFU for these samples and compared the *S. aureus*–positive samples ($n = 3$ patients) with patients harboring low bacteria colonization (<10^4 CFU/cm^2) as controls ($n = 5$ patients). Figure 3F and table S1 show the change in fluorescence intensity of stained DNAgel coincubated with the wound culture supernatant after 24 hours. Whereas DNAgel exposed to the *S. aureus*–positive samples exhibited more than 52% decrease in fluorescence intensity in the test group, the fluorescence intensity of DNAgel exposed to control samples decreased by no more than 27%. These results suggest that DNAgel is degraded in the presence of *S. aureus* and the hydrolysis of DNAgel by other wound-colonizing microbes is minimal.

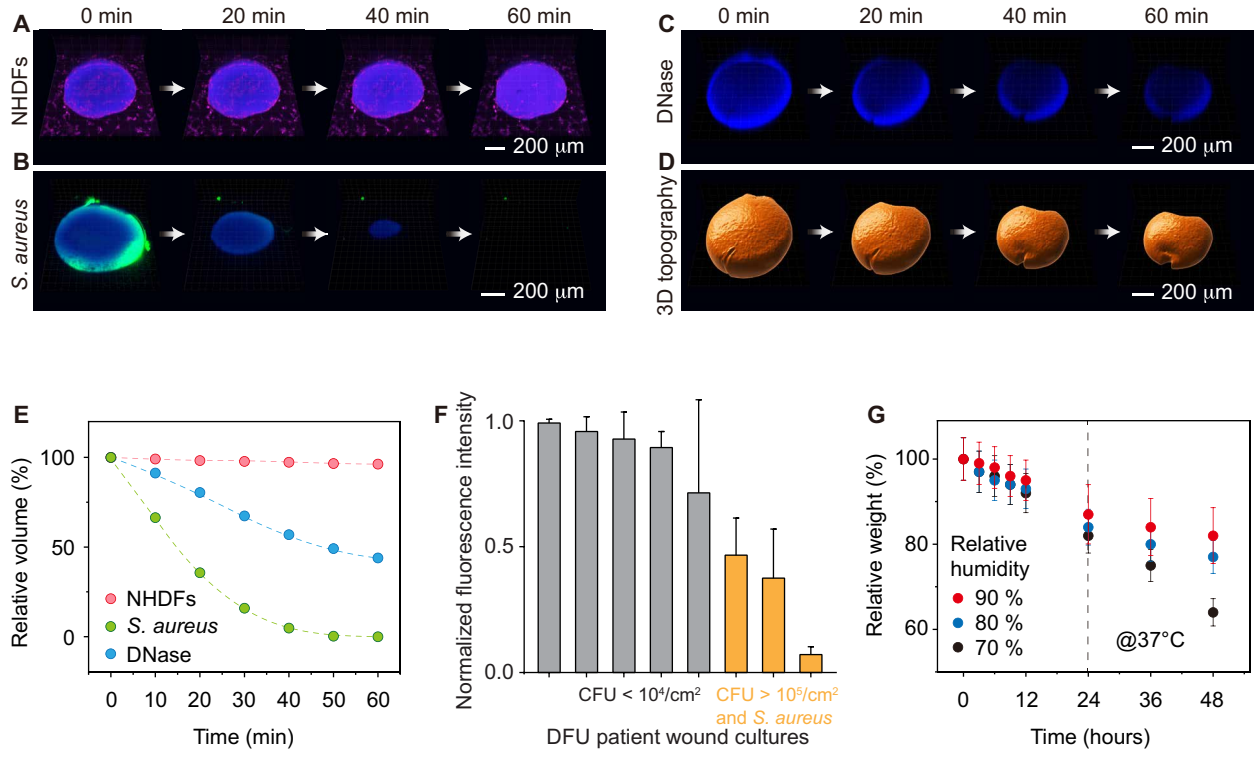

Fig. 3. DNAgel bacterial response. (**A** to **C**) Confocal fluorescence images of DNAgel coincubated with live neonatal human dermal fibroblasts (NHDFs; ~2×10^4 cells) (A), *S. aureus* (~7×10^7 CFU) (B), and DNase (1 U/μl) (C). DNAgel is stained using NucBlue (blue). NHDFs are stained using CellMask (purple), and *S. aureus* are stained using the BacLight Kit (green). (**D**) 3D topographic reconstruction of image in (C). (**E**) Relative volume change corresponding to the 3D images in (A) to (C). (**F**) Fluorescence intensity of DNAgel coincubated for 24 hours with culture supernatant of wound swab cultures from diabetic foot ulcer (DFU) patients. Error bars show means ± SD ($n = 3$ replicates). DNAgel is stained using SYBR Gold. (**G**) Relative weight change of DNAgel under different relative humidity at 37°C over 48 hours.

We also characterized the dehydration properties of DNAgel by placing 0.5 g of hydrogel in an opened centrifuge tube exposed to an environment with constant temperature (37°C) and controlled relative humidity. The hydrogel maintains more than 80% weight at 70% relative humidity after 24 hours (Fig. 3G), which demonstrates a substantially longer dehydration time compared to common hydrogels such as κ-carrageenan/polyacrylamide hydrogel that retain only 30% weight after exposure to similar conditions (*42*). This anti-dehydration property of DNAgel can be partially attributed to the hydrophilic poly(ethylene glycol) in the crosslinker. The dehydration time represents a lower bound for the lifetime of DNAgel because moisture is typically maintained in the wound environment by a wide range of wound dressings (fig. S5). However, additional studies will be needed to establish functional lifetime across the range of wound conditions, dressing types, and surrounding environment relevant to clinical applications.

Permittivity tunability and biocompatibility of DNAgel

Incorporating DNAgel with conductive dopants can increase sensitivity of the radio frequency response to biological stimuli. We evaluated the tunability of dielectric permittivity of DNAgel by incorporating five different conductive dopants in the hydrogel network: poly(3,4-ethylenedioxythiophene)–poly(styrene sulfonate) (PEDOT:PSS), $Ti_3C_2T_x$ MXene, graphene oxide (GO_x), single-walled carbon nanotube (SWCNT), and silver nanowire (AgNW) (Fig. 4, A and B). The biocompatibility of dopants was first examined by coincubating DNAgels with NHDFs for 48 hours (Fig. 4C). Pristine DNAgel exhibited excellent biocompatibility with cell viability, assessed using trypan blue staining, similar to controls (Fig. 4D). The presence of conductive nanoparticles or polymers resulted in reduction of the cell viability, although dopant cytotoxicity was reduced after incorporation into DNAgel network (fig. S6), which highlights the biocompatibility of the pristine DNAgel. We characterized the permittivity of doped DNAgels and found that AgNW can render a permittivity 1.47 times higher than that of pristine DNAgel within the tested bandwidth (1 to 200 MHz) (Fig. 4E). Figure 4F shows a radar plot of the achievable range of biocompatibility and permittivity for the different dopants. For a viability threshold of 80% (fig. S6), GO_x and $Ti_3C_2T_x$ MXene can achieve 29.5 and 28.6% increase in average dielectric permittivity, respectively. Nevertheless, we chose to use pristine DNAgel for this study due to its nontoxicity and sufficient permittivity for robust infection detection.

Design and optimization of the capacitive sensing structure

To establish an interface for signal transduction, we designed a capacitive sensing structure consisting of an interdigitated electrode pattern on a flexible polyimide coated with DNAgel (Fig. 5A). Finite element simulations show the effect of the gap between electrodes d, the thickness of the DNAgel layer t_1, and the thickness of the SU-8 layer t_2 on the sensor capacitance. As d is reduced from 350 to 50 μm, the intensity of the electric displacement field $\boldsymbol{D}$ fringing above the electrodes increases (Fig. 5B), which results in higher

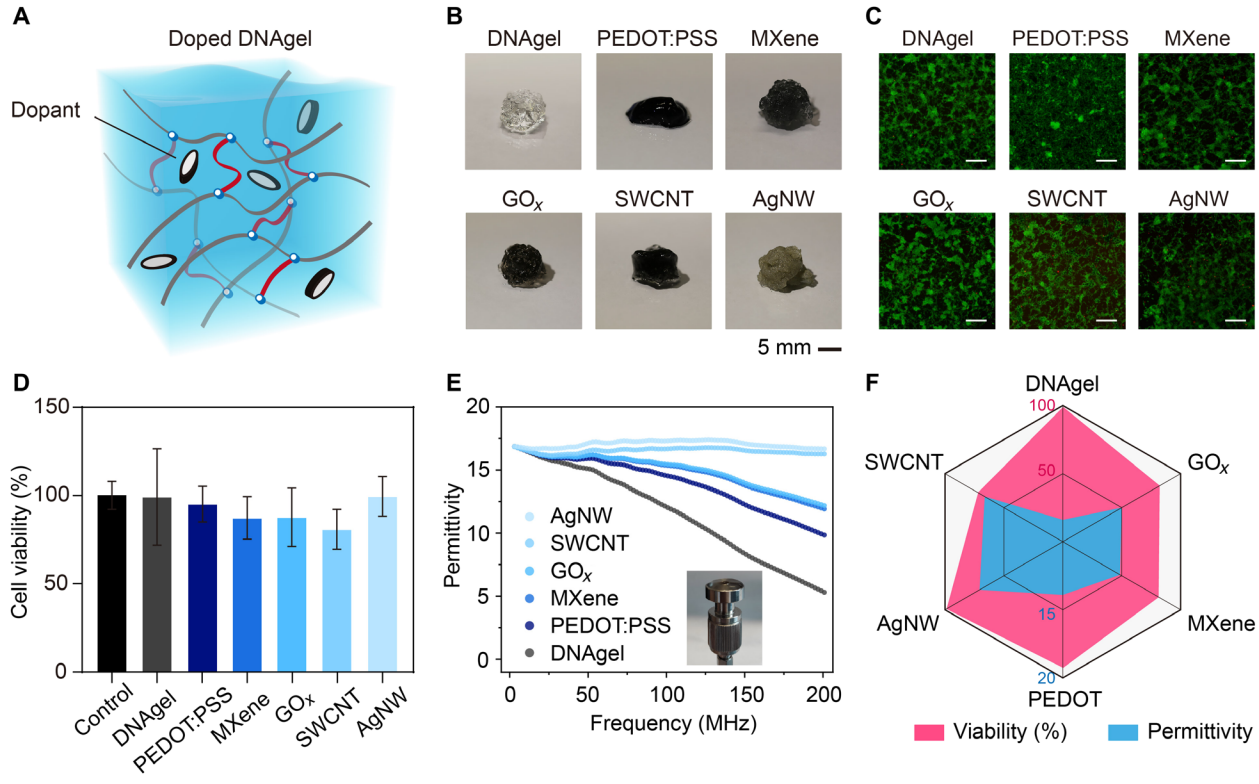

Fig. 4. DNAgel tunability and biocompatibility. (**A**) Illustration of DNAgel with dopant embedded in its 3D network. (**B**) Images of DNAgels synthesized without dopants, and with poly(3,4-ethylenedioxythiophene)-poly(styrene sulfonate) (PEDOT:PSS), $Ti_3C_2T_x$ MXene, graphene oxide (GO_x), single-walled carbon nanotube (SWCNT), and silver nanowire (AgNW). (**C**) Fluorescent images of NHDFs after 48 hours of coincubation with the DNAgels. Scale bars, 500 μm. (**D**) Viability of NHDFs after 48 hours of coincubation with the DNAgels. Error bars show means ± SD ($n = 3$ samples). (**E**) Dielectric permittivity of DNAgels. Inset shows dielectric probe for permittivity measurement. (**F**) Radar plot of the viability and permittivity for the DNAgels. Photo credit: Z. Xiong, National University of Singapore.

capacitance and sensitivity to the presence of the DNAgel layer. Figure 5C displays an overview of these parameters by showing a stacked contour plot of sensor capacitance, as a function of d, t_1, and t_2. With a specific DNAgel thickness, a smaller electrode gap and thinner SU-8 can boost the capacitance induced by hydrogel. On the basis of the optimization result, we choose d = 250 μm, t_1 = 1 mm, and t_2 = 2 μm as the sensor parameters, which yield a capacitance of ~0.15 pF/mm^2.

We numerically analyzed three electrode configurations (Fig. 5D and fig. S7) and selected the design with ~15 mm^2 active area for subsequent use, unless otherwise stated. The interdigitated structures were fabricated through a printing-and-etching process on a flexible printed circuit board (see Materials and Methods). Cross-sectional images of the electrodes showed conformal coating of SU-8 over the copper (Cu) surface (Fig. 5E), which protects Cu electrodes and prevents potential cytotoxicity. A circuit comprising an *LC* tank and a half-wave rectifier was used to convert the capacitance signal into a voltage output V_{out} (Fig. 5F). The resonant frequency of the *LC* tank was set as 13.56 MHz, in alignment with the frequency for NFC communication. We characterized the response of the sensing circuit by gradually decreasing the coverage area of DNAgel from ~15 to 0 mm^2 to mimic digestion by DNase. The circuit exhibited a change in the input impedance from $Z_{in} = 8.5 + 30.3j$ to $Z_{in} = 42.5 + 42.6j$, resulting in a ~0.7-MHz shift in the resonant frequency (Fig. 5, G and H) and an ~0.25-V increase in V_{out} (Fig. 5I and fig. S8) (*43*–*45*).

In vitro and in vivo detection of *S. aureus*

WINDOW integrates the DNAgel capacitive sensor and front-end circuit with an NFC module (fig. S9) to enable battery-free and wireless data transmission through wound dressings. The wireless design uses two coils, the first for the *LC* biosensing module and the second for the NFC module, which have an optimized spacing between the coils of 3.5 mm (fig. S10). Figure S11 shows that the coil design achieves stable transmission to an external reader except under extreme misalignments. WINDOW can be mounted on curved body surfaces by wound dressings, exhibiting negligible (±0.01 V) fluctuation in the readout signal when the bending angle is changed from 180° to 60° (Fig. 6A). The wireless readout of the sensor is highly reproducible, as DNAgel coverage is varied from 0 to 100% (Fig. 6B).

We evaluated the response of WINDOW to *S. aureus* using the sterile-filtered culture supernatant. For in vitro experiments, WINDOW was attached to gauze (1 × 1 cm^2) permeated with filter-sterilized (0.22-μm filter) *S. aureus* culture supernatant at various concentrations at room temperature. The sensor was fixed by a Tegaderm film (3M) and wirelessly recorded via a smartphone over 48 hours. Whereas control samples exposed to culture medium resulted in no signal change after 24 hours, samples containing *S. aureus* culture supernatant produced a signal increase of 0.15 V for the 10^5 CFU group and 0.38 V for the 10^6 CFU group (Fig. 6C). Figure S12 shows the dose-response curve of the sensor after 24 hours.

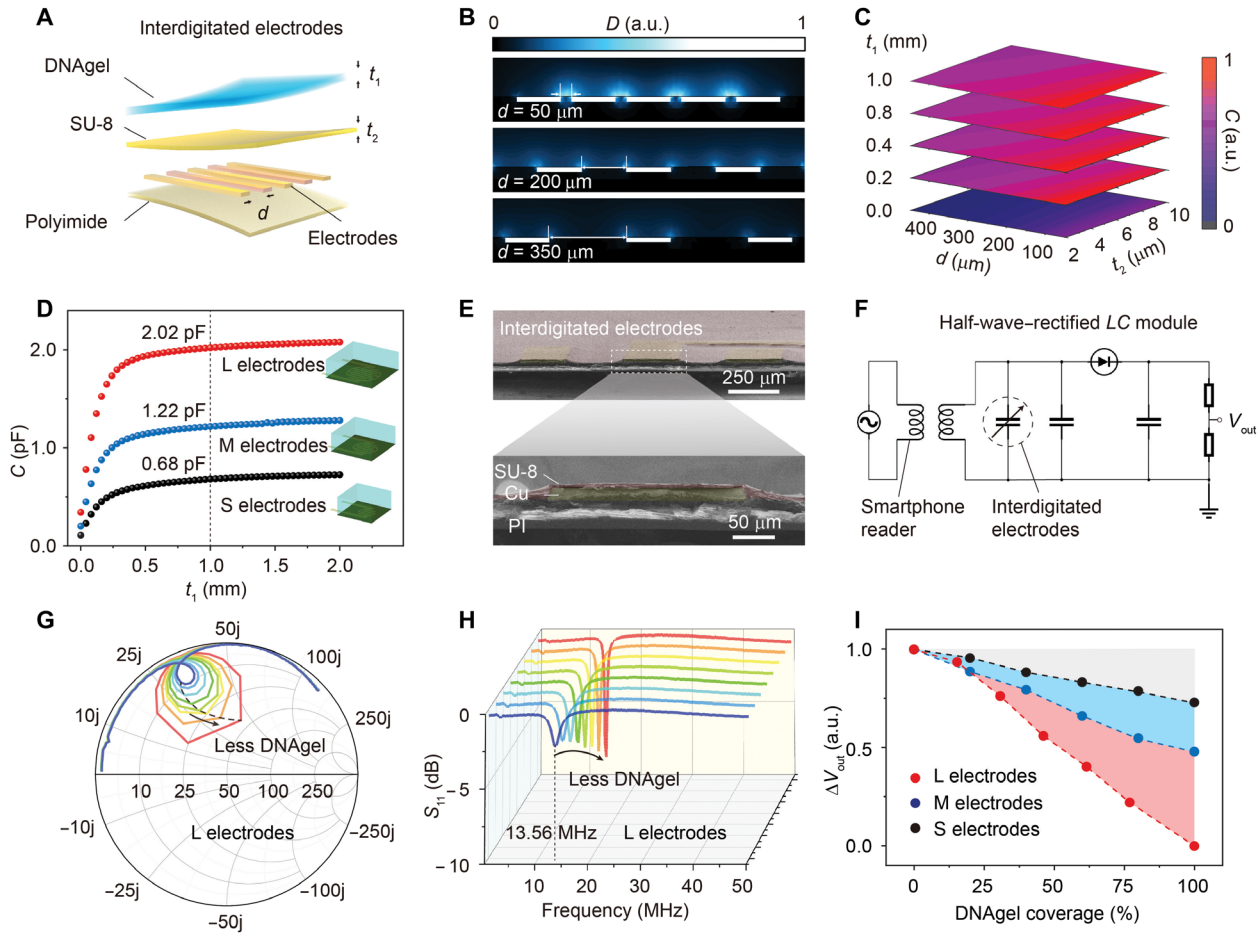

Fig. 5. WINDOW design and characterization. (**A**) Schematic of the capacitive sensing structure comprising an interdigitated electrode pattern with DNAgel in the region of the fringing electric field. The parameters are the gap between electrodes (d), the DNAgel thickness (t_1), and the SU-8 thickness (t_2). (**B**) Electric displacement field D for interdigitated electrodes with varying gaps. a.u., arbitrary units. (**C**) Contour plots of the capacitance of electrodes as a function of d, t_1, and t_2 normalized to the capacitance with $d = 50$ μm, $t_1 = 1$ mm, and $t_2 = 2$ μm. (**D**) Capacitance as a function of DNAgel thickness for electrodes with different areas. The areas are 15 mm^2 (L), 8 mm^2 (M), and 3.5 mm^2 (S) with $d = 250$ μm and $t_2 = 2$ μm. (**E**) Colored scanning electron microscope image of the cross-section of electrodes. PI, polyimide. (**F**) Diagram of the circuit of biosensing module. Changes in the capacitive electrodes detune the *LC* circuit, resulting in a change in the output voltage (V_{out}). (**G**) Smith chart of the *LC* circuit as the DNAgel coverage decreases from 100% to 0%. The frequency range is from 0.5 to 50 MHz. (**H**) Reflection coefficient S_{11} of the *LC* circuit as the DNAgel coverage decreases from 100% to 0%. (**I**) Relative change in output voltage of the biosensing modules as a function of DNAgel coverage.

WINDOW produces a detectable signal when the amount of *S. aureus* exceeds 10^5 CFU, which is at the lower end of clinical thresholds (10^5 to 10^6 CFU) widely used for laboratory diagnosis of infection (*46*). For amounts of *S. aureus* greater than 10^7 CFU, the sensor response saturates at about 0.45 V due to complete degradation of DNAgel, thereby providing binary detection of infection. These results indicate that the sensor can detect secretory DNase activity when the amount of *S. aureus* approaches or exceeds thresholds for clinical infection.

We next demonstrated the ability of WINDOW to detect wound infection in vivo using an acute wound model in mice (*47*). Full-thickness excisional bilateral wounds (~6 mm in diameter) through the panniculus carnosus were created on the dorsum with randomly assigned control and test sites (Fig. 6D). A piece of gauze with live *S. aureus* suspension (10^5 or 10^6 CFU) or sterile tryptic soy broth (TSB) was attached to the wound followed by placement and fixation of the sensor using adhesive dressings. Infected wounds with WINDOW showed similar wound conditions as the uninfected control wounds after 24 hours (Fig. 6E). All sensors remained attached to the wound, and mice with the sensors did not show observable behavioral differences compared to controls (Fig. 6F and movie S4). No obvious infection-related clinical signs, such as erythema, suppuration, and friable granulation tissue, were identified in both wounds. Wound culture at the experimental end point confirmed that *S. aureus* infection was established in the test groups (>10^6 CFU/ml for both the 10^5 and 10^6 CFU groups) (Fig. 6G). Trace amounts of *S. aureus* (~10^5 CFU/ml) were also measured in the control (TSB) group, which can be attributed to *S. aureus* normally present on the skin and variations due to handling. Using a custom app, signals from WINDOW were conveniently extracted by placing a smartphone in close proximity to the wound dressing (movie S5). Wounds with live *S. aureus* (10^5 and 10^6 CFU) exhibited a 0.4-V change in signal after 24 hours (Fig. 6H), triggering an infection alert on the smartphone (Fig. 6I).

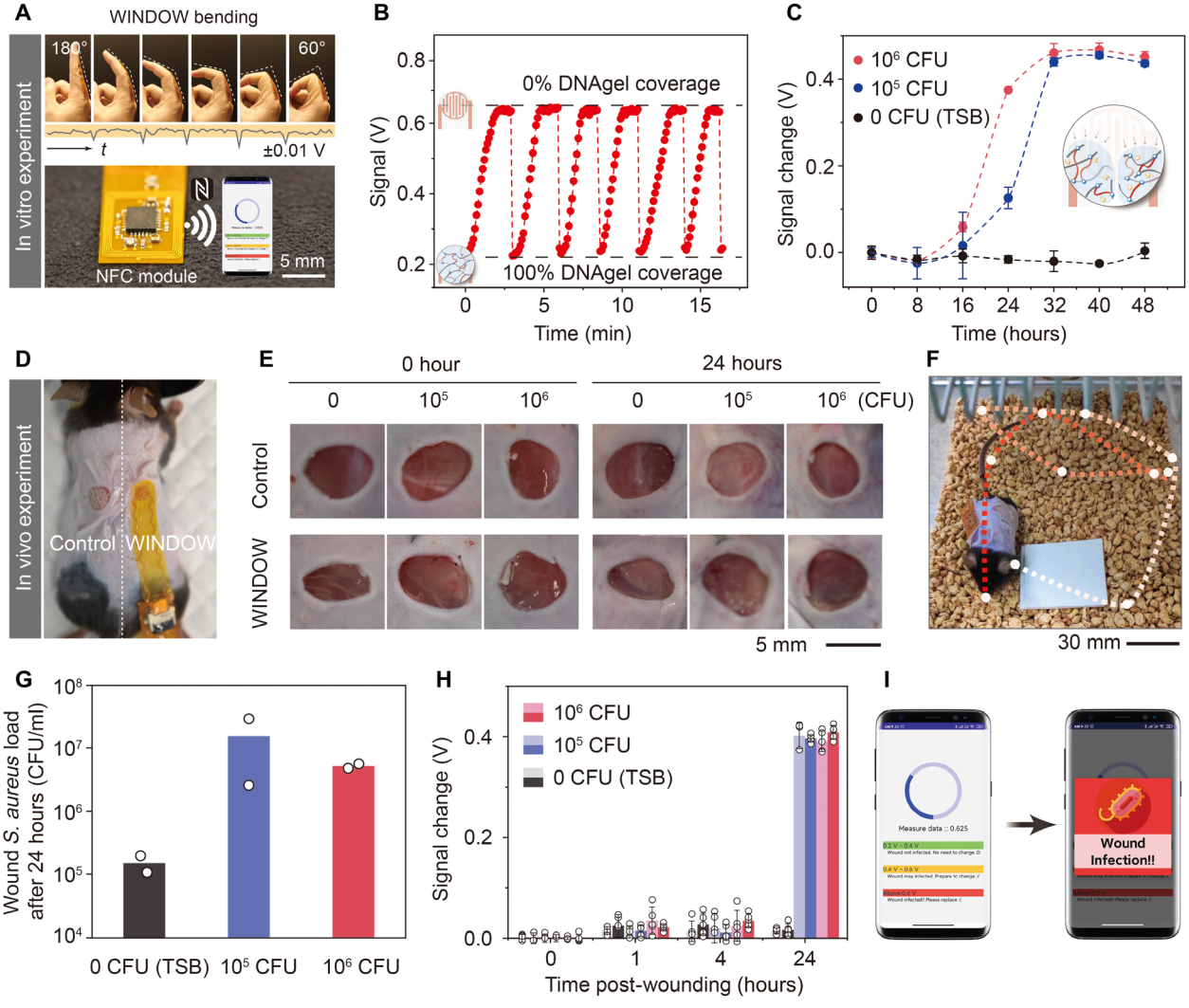

Fig. 6. Infection detection with WINDOW. (**A**) A WINDOW mounted on the index finger. The yellow region shows the readout signal corresponding to the bending angles indicated by the dotted white lines. Inset: Image of the NFC module. (**B**) Signal readout by a smartphone as the area of the capacitor covered by DNAgel is varied. (**C**) Signal change when WINDOW is exposed to *S. aureus* culture supernatant at room temperature over 48 hours. Error bars show means ± SD ($n = 5$ data points). (**D**) WINDOW mounted on a skin wound in vivo under transparent wound dressing. Left flank wound is used as control. (**E**) Images of wounds applied with TSB or live *S. aureus* suspension (10^5 and 10^6 CFU) immediately after wounding (0 hour) and 24 hours after wounding. Images are representative from each group ($n = 2$ mice per group). (**F**) Freely moving mouse carrying WINDOW 24 hours after wounding. Dashed line shows the motion trajectory over 30 s. (**G**) *S. aureus* load at the wound site established by wound culture 24 hours after wounding. (**H**) Signal change recorded by smartphone for each group. Error bars show means ± SD ($n = 5$ wireless measurements). (**I**) Smartphone interface displaying signal acquisition and detection of wound infection. Photo credit: Z. Xiong, National University of Singapore.

DISCUSSION

We have proposed and demonstrated WINDOW, a flexible, wireless, and battery-free sensor based on DNAgel that can interface with wounds and detect infection. WINDOW exploits material formulations, fabrication approaches, circuit layouts, and wireless techniques that collectively enable DNase activity associated with *S. aureus* virulence activity to be transduced into a wireless signal detectable by a smartphone. In vitro experiments establish that the sensor responds selectively to amounts of *S. aureus* near to thresholds for clinical infection (10^6 CFU or more per gram of viable tissue) in both culture supernatant and clinical wound exudates from DFUs (*46*). In vivo studies in a mouse wound model further demonstrate the utility of WINDOW to detect clinically relevant amounts of *S. aureus* when interfaced with wounds for 24 hours.

Beyond detecting *S. aureus*, we postulate that WINDOW can be used to detect secreted DNases from other wound-associated pathogens such as *P. aeruginosa* and *S. pyogenes* (*36*). Although *S. aureus* and other bacteria commonly implicated in wound infections can be isolated from unaffected skin in many patients, they have markedly lower abundance and expression of virulence factors on sites where the epidermis is not breached (*48*, *49*). Consequently, the presence of these and other skin commensal bacteria is not expected to substantially affect the signal reported by the sensor. Nevertheless, further clinical investigations of the wound microbial composition

together with WINDOW's performance on human wounds are needed to determine whether secreted DNase activity can serve as a general biomarker for infections. Possible effects of other virulence factors on the response of DNAgel should also be carefully investigated.

Future work may expand the functionality of DNAgel for wound monitoring. Depending on the wetness of the wound environment, dehydration of DNAgel can limit time duration over which the sensor is effective. Material engineering strategies may improve the anti-dehydration properties of DNAgel. For example, bonding a thin elastomer film to hydrogel has been shown to greatly increase anti-dehydration (*50*), and adding microfluidic structures can constrain dehydration while helping to dissipate liquified gel after enzymatic degradation (*39*, *51*). Using CRISPR-associated nucleases, DNAgel degradation actuated by specific RNA inputs have also been recently demonstrated, which could be exploited as a detection mechanism for pathogens not associated with DNase (*52*). The sensitivity of DNAgel is presently limited by the cytotoxicity of conductive dopants (*53*–*55*). Systematic exploration of biocompatible dopants, such as coated inert gold particles (*56*), could also yield approaches to increase sensitivity.

Clinically, the sensor could be embedded in wound dressing to enable patients to monitor their wounds between clinical assessments and seek appropriate intervention in the event that infection is detected. Future work will focus on technological developments to provide additional capabilities for wound care. For example, in addition to detecting infection, quantitative assessment of infection severity could be valuable in helping to determine the appropriate treatment at the point of care. In this aspect, existing sensors for measuring wound temperature, moisture, and pH (*20*, *57*) as well as specific biomarkers could be integrated with the device to provide multiplexed analysis. Alternative wireless technologies could also be used to enable passive streaming of data from the sensor without requiring patients to bring a smartphone in proximity to the wound. This mode of operation requires the sensor to have a power supply, which may be addressed using a combination of solutions for energy storage, wireless charging, and energy harvesting (*58*–*60*).

MATERIALS AND METHODS

DNAgel synthesis

DNA strands were covalently crosslinked using poly(ethylene glycol) diglycidyl ether (PEGDE) to form a 3D hydrogel network. The hydrophilic poly(ethylene glycol) component of PEGDE confers increased anti-dehydration and biocompatibility, while the two epoxide groups in PEGDE react with primary amine groups on the adenosine, guanine, and cytosine nucleotide bases and bonds adjacent DNA strands (*61*, *62*). Specifically, DNAgel precursor was prepared by dissolving 10 weight % (wt %) deoxyribonucleic acid sodium salt (smDNA) in 4.0 mM NaBr solution at room temperature. Crosslinker (2.5 wt %), PEGDE (M_n = 500), was uniformly mixed with the precursor. *N*,*N*,*N*′,*N*′-Tetramethylethylenediamine (TMEDA; 0.5 wt %), as the catalyst, was further mixed with the hydrogel precursor. The precursor can be printed onto planar/curved surface or casted into macro/micromold and kept under 90% relative humidity for 48 hours to complete the crosslinking reaction. To speed up the reaction, the precursor can be transferred into a sealed centrifuge tube and immersed in a water bath at 85°C for 2 hours to complete the gelation. After gelation, the prepared DNAgel was thoroughly rinsed by deionized (DI) water to remove unreacted chemicals. All DI water used in the experiment was from a Barnstead Nanopure ultrapure water system (Thermo Fisher Scientific).

Bioresponse and anti-dehydration of DNAgel

Wound isolate *S. aureus* ATCC 29213 (SA29213) from a streak plate was inoculated into 10 ml of sterilized TSB (Sigma-Aldrich) and allowed to grow overnight at 37°C at 200 rpm. The CFU of *S. aureus* was characterized by optical density (OD) using a spectrometer. NHDFs were incubated in the medium composed of Dulbecco's modified Eagle's medium (Thermo Fisher Scientific) + 10% fetal bovine serum + 1% penicillin-streptomycin at 37°C in a humidified atmosphere (5% CO_2). DNase (3000 U/ml; Nuclease S7, Sigma-Aldrich) stock was prepared using 0.5 mM $CaCl_2$ solution (sterilized by 0.22-μm filter). All stocks were further diluted by corresponding medium before imaging. To make a fair evaluation of selectivity, the total cellular numbers of NHDFs and *S. aureus* were determined on the basis of an assumption that the effective metabolites produced by NHDFs and *S. aureus*, for instance, DNase, are equivalent per unit cell volume. Given the volume of fibroblast (~2000 μm^3) and *S. aureus* (~0.52 μm^3) (*63*), the total cellular volume of NHDFs (~2×10^4 cells, 4×10^7 μm^3) and *S. aureus* (~7×10^7 CFU, 3.7×10^7 μm^3) are comparable, therefore confirming the selective response of DNAgel.

For the imaging, DNAgel samples were transferred into a chambered borosilicate coverglass system (Lab-Tek, Thermo Fisher Scientific). Fluorescent images were acquired with a confocal microscope (Zeiss LSM 710) in *Z*-stack mode with controlled ambient by Zeiss incubation system. 3D topography of fluorescent images was reconstructed by Imaris package (Oxford Instruments). A bacterial viability stain (LIVE/DEAD BacLight Bacterial Viability Kit, Invitrogen, Thermo Fisher Scientific) was used for *S. aureus*, a plasma membrane stain (CellMask, Invitrogen, Thermo Fisher Scientific) for NHDFs, and a fluorescent stain (NucBlue, Invitrogen, Thermo Fisher Scientific) for DNAgel and NHDF nuclei. The dehydration tests were performed in a chamber (SH-262, ESPEC) with controlled temperature and relative humidity.

In vitro degradation of DNAgel by *S. aureus* and skin commensal bacteria strains

DNAgel was prepared as described above. SYBR Gold Nucleic Acid Stain (Invitrogen, Thermo Fisher Scientific) was added to the gel precursor immediately after the addition of TMEDA and mixed uniformly. Twenty-five microliters of precursor drops was placed onto the lids of 150-mm tissue culture–treated dishes (Corning), sealed with parafilm, and kept away from light for 48 hours for complete crosslinking. The crosslinked DNAgel was then washed thoroughly with ultrapure water (Merck Millipore).

Cultures of ATCC bacterial strains were grown for 24 hours in TSB at 37°C. The OD at 600 nm (OD_{600}) of each culture was noted. The cultures were then centrifuged (5000*g*, 10 min, 4°C), sterile-filtered (0.22 μm filter), and stored at −20°C until needed. Twenty-five microliters of sterile-filtered culture supernatant was added to each DNAgel drop and incubated at 37°C for 24 hours. Positive controls (DNase I, Zymo Research) and negative controls (sterile TSB) were also set up.

DNAgel drops were imaged immediately after addition of culture supernatants and after 24 hours of incubation, using the Gel Doc EZ Imager and UV Tray (Bio-Rad). The change in size and fluorescence intensity of each DNAgel drop was quantified with ImageJ. Experiments were performed in technical triplicates.

DNAgel response to patient wound samples

Wound sampling from DFU patients was approved by St Luke's Hospital Institutional Review Board (IRB-02-2019-08-28), and all subjects provided written consent before participation. The inclusion criteria for this study comprised male/female individuals >21 years old who (i) have received a clinical diagnosis of diabetes, (ii) are able to provide consent, and (iii) have one or more DFUs present on the lower limb. Patients who were involved in other interventional clinical trials were excluded from this study. The wounds were cleansed with sterile water before sampling, and one sterile Levine swab was used to collect the wound fluid and microbes from each patient before debridement. Five hundred microliters of 50 mM tris (pH 6) with 5 mM $CaCl_2$ was added to each swab on the same day the swab was collected and vortexed for 30 s. One hundred microliters of the sample was mixed with 400 μl of TSB containing 15% glycerol and stored at −80°C in aliquots until further processing. For 18 patient samples with available clinical microbiology reports, we determined the CFU count. Ten microliters of the sample was thawed, diluted, and plated onto TSB agar plates and incubated for 48 hours before a manual count was done (in triplicates). Samples with *S. aureus* (three patients, $>10^4$ CFU/cm^2) and low microbial colonization (five patients, without *S. aureus*, $<10^4$ CFU/cm^2) were selected for DNAgel test. To assess DNase hydrogel degradation, 10 μl of each sample was added to 4 ml of TSB and incubated for 24 hours at 37°C with shaking at 200 rpm. The culture supernatant was obtained by centrifuging the culture at 5000 rpm for 5 min and then filtered with 0.22-μm filters. The DNAgel degradation assay was performed as per the cultured bacteria strains above.

DNAgel doping and characterization

$Ti_3C_2T_x$ MXene nanosheets were prepared according to the literature. Lithium fluoride (LiF) (1.0 g; ≥99.0%; Sigma-Aldrich, BioUltra) was added to 6.0 M hydrochloric acid (HCl; 37%; Sigma-Aldrich, ACS reagent) solution (20 ml) under vigorous stirring. After the dissolution of LiF, 1.0 g of Ti_3AlC_2 powder (Tongrun Info Technology Co. Ltd.) was added slowly into the hydrogen fluoride (HF)-containing solution, and the mixture was then kept at 35°C for 24 hours. Thereafter, the solid residue was washed with DI water several times until the pH value increased to ca. 7.0. Subsequently, the washed residue was added into 100 ml of DI water (Millipore), ultrasonicated for 1 hour under N_2 atmosphere, and centrifuged at 3000 rpm for 30 min. The supernatant was collected as the suspension of $Ti_3C_2T_x$ MXene nanosheets.

$Ti_3C_2T_x$ MXene (0.2 wt %), GO_x (Timesnano), PEDOT:PSS (Clevios PH 1000, Heraeus), SWCNTs (Timesnano), and AgNWs (50 nm in diameter; Kechuang Advanced Materials) were doped into hydrogel precursor, respectively. The gelation was completed following the protocol of undoped hydrogel. After the gelation, the permittivity of hydrogels was obtained using a dielectric probe (85070E, Keysight) and a vector network analyzer (N9923A FieldFox, Keysight) after calibration by DI water.

To evaluate the cytotoxicity of dopants, ~1 μl of DNAgel and dopants (1 wt %) were spiked into 50 μl of NHDFs (~4×10^4 cells) and incubated for 48 hours. The NHDFs were then observed under a microscope (Nikon Eclipse Ti2 microscope) after treatment with the LIVE/DEAD Cell Imaging Kit (Invitrogen, Thermo Fisher Scientific). For viability results, 50 μl of NHDFs (~4×10^4 cells) was incubated with ~1 μl of DNAgel and dopants (1 wt %) for 48 hours and tested through trypan blue staining and standard 3-(4,5-Dimethylthiazol-2-yl)-2,5-diphenyltetrazolium bromide (MTT) assay.

WINDOW design and fabrication

Interdigital capacitive sensing electrodes were modeled by using more than 2.48×10^6 tetrahedrons and simulated by the finite-difference time-domain method (CST Microwave Studio, Dassault Systems) to evaluate the capacitive sensing performance. The optimization was realized through systematically sweeping key geometrical parameters. Mutual coupling analysis was conducted by CST with circuit layout from Altium Designer.

The interdigitated electrodes were fabricated by printing (ColorQube 8880, Fuji Xerox) the traces (fig. S7) on a copper-polyimide substrate (18-μm-thick copper, 25-μm-thick polyimide layer; DuPont). After baking at 70°C for 10 min, the printed substrate was etched using H_2O_2 and HCl and cleaned by immersion in hexane and ethanol to yield the patterned traces. SU-8 was coated and ultraviolet (UV) crosslinked over the sensor surface as protection layer with a thickness of ~2 μm. A crescent silicone pillar (~1 mm in thickness) was added onto the capacitive sensor for mechanical support, followed by DNAgel functionalization (~1 mm in thickness) of the active region of the sensor. The circuit diagram for NFC module and the electronic components involved can be found in fig. S9.

In vitro evaluation of WINDOW

Culture supernatant of SA29213 was used for in vitro test. SA29213 was grown overnight on tryptic soy agar (Sigma-Aldrich). Single colony of SA29213 was inoculated in TSB (Sigma-Aldrich) and allowed to grow to OD_{600} = 0.8 at 37°C. TSB was then inoculated (OD_{600} = 0.01) and cultured at 37°C overnight. Overnight culture, with tested CFU number, was clarified via centrifugation (3000*g*, 30 min, 4°C), sterile-filtered (0.22-μm filter), and stored at −20°C until needed. For in vitro experiment, culture supernatant was diluted by TSB as an equivalent substitute for live *S. aureus* suspension with effective secretory DNase. The hydrogel coverage response was recorded with a mixed domain oscilloscope (MDO3012, Tektronix) and a vector network analyzer (N9923A FieldFox, Keysight).

In vivo evaluation of WINDOW

Male C57 black 6 inbred mice (C57BL/6) between 8 and 10 weeks of age and 25 and 30 g of weight were used. Mice were provided by in-house colony by the animal facility of Lee Kong Chian (LKC) School of Medicine. The skin on the back of the mice was prepared by shaving and applying depilatory cream (Nair). The injury site was then wiped three times with 70% ethanol. Surgery was performed under inhaled isoflurane (2 to 5%), and depth of anesthesia was checked by testing pedal reflex. Buprenorphine (1.5 mg/kg) was injected subcutaneously before wounding for sustained pain relief. Full-thickness excisional wounds through the panniculus carnosus were achieved by lifting the back skin of the mice from the dorsum and making an incision with a 6-mm punch biopsy (Acuderm Inc.). The two bilateral wounds equidistant from the midline and spaced either side of the dorsum were randomly assigned as the control wound or the test wound for WINDOW application.

Mice were divided into three groups, where test wounds were applied with either TSB or live bacteria suspension of SA29213 at 10^5 or 10^6 CFU (n = 2 mice per group). Overnight *S. aureus* culture was diluted with TSB to achieve target CFU numbers for the experiment. Gauze was overlaid onto the wound, and 20 μl of bacteria

suspension/TSB was applied directly onto the gauze and wound. DNAgel-functionalized WINDOW was then placed onto the gauze and fixed by a small piece of Tegaderm film (3M). The whole back of the mice was then covered with an OPSITE dressing (Smith & Nephew) to ensure that both the WINDOW and gauze remained in place. A mobile phone with a custom app was used to record the signal 0, 1, 4, and 24 hours after WINDOW attachment. To quantify the amount of bacteria 24 hours after wounding, mice skin surrounding the wound was sampled (approximately 1 cm × 1 cm) and placed in pre-weighed 2-ml microcentrifuge tubes containing 1 ml of sterile phosphate-buffered saline. The mice skin sample was weighed and sonicated in a chilled sonicator (Elmasonic S 30 H, Elma Schmidbauer GmbH, Germany) to dissociate adherent bacteria (37 kHz, 10 min per cycle, three cycles, 1-min vortex after each cycle). Bacteria in each sample were enumerated via CFU counting and normalized by sample weight. All experiments conformed to the *Guide for the Care and Use of Laboratory Animals* published by the National Institutes of Health, USA, and protocol approved by the Institutional Animal Care and Use Committee (IACUC) of the Animal Research Facility of Nanyang Technological University, with consideration to ethical use and animal welfare.

SUPPLEMENTARY MATERIALS

Supplementary material for this article is available at https://science.org/doi/10.1126/sciadv.abj1617

View/request a protocol for this paper from *Bio-protocol*.

REFERENCES AND NOTES

1. M. Mehrali, S. Bagherifard, M. Akbari, A. Thakur, B. Mirani, M. Mehrali, M. Hasany, G. Orive, P. Das, J. Emneus, T. L. Andresen, A. Dolatshahi-Pirouz, Blending electronics with the human body: A pathway toward a cybernetic future. *Adv. Sci.* **5**, 1700931 (2018).
2. C. Xu, Y. Yang, W. Gao, Skin-interfaced sensors in digital medicine: From materials to applications. *Matter* **2**, 1414–1445 (2020).
3. T. Stuart, L. Cai, A. Burton, P. Gutruf, Wireless and battery-free platforms for collection of biosignals. *Biosens. Bioelectron.* **178**, 113007 (2021).
4. R. Lin, H.-J. Kim, S. Achavananthadith, S. A. Kurt, S. C. C. Tan, H. Yao, B. C. K. Tee, J. K. W. Lee, J. S. Ho, Wireless battery-free body sensor networks using near-field-enabled clothing. *Nat. Commun.* **11**, 444 (2020).
5. S. R. Madhvapathy, H. Wang, J. Kong, M. Zhang, J. Y. Lee, J. B. Park, H. Jang, Z. Xie, J. Cao, R. Avila, C. Wei, V. D'Angelo, J. Zhu, H. U. Chung, S. Coughlin, M. Patel, J. Winograd, J. Lim, A. Banks, S. Xu, Y. Huang, J. A. Rogers, Reliable, low-cost, fully integrated hydration sensors for monitoring and diagnosis of inflammatory skin diseases in any environment. *Sci. Adv.* **6**, eabd7146 (2020).
6. S. Niu, N. Matsuhisa, L. Beker, J. Li, S. Wang, J. Wang, Y. Jiang, X. Yan, Y. Yun, W. Burnett, A. S. Y. Poon, J. B. H. Tok, X. Chen, Z. Bao, A wireless body area sensor network based on stretchable passive tags. *Nat. Electron.* **2**, 361–368 (2019).
7. Y. Song, J. Min, Y. Yu, H. Wang, Y. Yang, H. Zhang, W. Gao, Wireless battery-free wearable sweat sensor powered by human motion. *Sci. Adv.* **6**, eaay9842 (2020).
8. J. Kim, J. R. Sempionatto, S. Imani, M. C. Hartel, A. Barfidokht, G. Tang, A. S. Campbell, P. P. Mercier, J. Wang, Simultaneous monitoring of sweat and interstitial fluid using a single wearable biosensor platform. *Adv. Sci.* **5**, 1800880 (2018).
9. C. K. Sen, G. M. Gordillo, S. Roy, R. Kirsner, L. Lambert, T. K. Hunt, F. Gottrup, G. C. Gurtner, M. T. Longaker, Human skin wounds: A major and snowballing threat to public health and the economy. *Wound Repair Regen.* **17**, 763–771 (2009).
10. P. G. Bowler, B. I. Duerden, D. G. Armstrong, Wound microbiology and associated approaches to wound management. *Clin. Microbiol. Rev.* **14**, 244–269 (2001).
11. V. Falanga, Wound healing and its impairment in the diabetic foot. *Lancet* **366**, 1736–1743 (2005).
12. P. Salvo, V. Dini, F. Di Francesco, M. Romanelli, The role of biomedical sensors in wound healing. *Wound Med.* **8**, 15–18 (2015).
13. S. E. Gardner, R. A. Frantz, B. N. Doebbeling, The validity of the clinical signs and symptoms used to identify localized chronic wound infection. *Wound Repair Regen.* **9**, 178–186 (2001).
14. A. R. Siddiqui, J. M. Bernstein, Chronic wound infection: Facts and controversies. *Clin. Dermatol.* **28**, 519–526 (2010).
15. N. Mehmood, A. Hariz, R. Fitridge, N. H. Voelcker, Applications of modern sensors and wireless technology in effective wound management. *J. Biomed. Mater. Res. B* **102**, 885–895 (2014).
16. W.-J. Deng, L.-F. Wang, L. Dong, Q.-A. Huang, LC wireless sensitive pressure sensors with microstructured PDMS dielectric layers for wound monitoring. *IEEE Sensors J.* **18**, 4886–4892 (2018).
17. Q. Pang, D. Lou, S. Li, G. Wang, B. Qiao, S. Dong, L. Ma, C. Gao, Z. Wu, Smart flexible electronics-integrated wound dressing for real-time monitoring and on-demand treatment of infected wounds. *Adv. Sci.* **7**, 1902673 (2020).
18. D. Sharp, Printed composite electrodes for in-situ wound pH monitoring. *Biosens. Bioelectron.* **50**, 399–405 (2013).
19. T. Guinovart, G. Valdés-Ramírez, J. R. Windmiller, F. J. Andrade, J. Wang, Bandage-based wearable potentiometric sensor for monitoring wound pH. *Electroanalysis* **26**, 1345–1353 (2014).
20. P. Mostafalu, A. Tamayol, R. Rahimi, M. Ochoa, A. Khalilpour, G. Kiaee, I. K. Yazdi, S. Bagherifard, M. R. Dokmeci, B. Ziaie, S. R. Sonkusale, A. Khademhosseini, Smart bandage for monitoring and treatment of chronic wounds. *Small* **14**, 1703509 (2018).
21. R. Rahimi, U. Brener, S. Chittiboyina, T. Soleimani, D. A. Detwiler, S. A. Lelièvre, B. Ziaie, Laser-enabled fabrication of flexible and transparent pH sensor with near-field communication for in-situ monitoring of wound infection. *Sensors Actuators B Chem.* **267**, 198–207 (2018).
22. S. D. Milne, I. Seoudi, H. Al Hamad, T. K. Talal, A. A. Anoop, N. Allahverdi, Z. Zakaria, R. Menzies, P. Connolly, A wearable wound moisture sensor as an indicator for wound dressing change: An observational study of wound moisture and status. *Int. Wound J.* **13**, 1309–1314 (2016).
23. T. R. Dargaville, B. L. Farrugia, J. A. Broadbent, S. Pace, Z. Upton, N. H. Voelcker, Sensors and imaging for wound healing: A review. *Biosens. Bioelectron.* **41**, 30–42 (2013).
24. H. J. Sismaet, A. Banerjee, S. McNish, Y. Choi, M. Torralba, S. Lucas, A. Chan, V. K. Shanmugam, E. D. Goluch, Electrochemical detection of pseudomonas in wound exudate samples from patients with chronic wounds. *Wound Repair Regen.* **24**, 366–372 (2016).
25. G. A. Zelada-Guillén, J. L. Sebastián-Avila, P. Blondeau, J. Riu, F. X. Rius, Label-free detection of staphylococcus aureus in skin using real-time potentiometric biosensors based on carbon nanotubes and aptamers. *Biosens. Bioelectron.* **31**, 226–232 (2012).
26. M. A. C. Stuart, W. T. S. Huck, J. Genzer, M. Müller, C. Ober, M. Stamm, G. B. Sukhorukov, I. Szleifer, V. V. Tsukruk, M. Urban, F. Winnik, S. Zauscher, I. Luzinov, S. Minko, Emerging applications of stimuli-responsive polymer materials. *Nat. Mater.* **9**, 101–113 (2010).
27. L. Hu, Q. Zhang, X. Li, M. J. Serpe, Stimuli-responsive polymers for sensing and actuation. *Mater. Horiz.* **6**, 1774–1793 (2019).
28. Y. Liu, J. Liu, S. Chen, T. Lei, Y. Kim, S. Niu, H. Wang, X. Wang, A. M. Foudeh, J. B. H. Tok, Z. Bao, Soft and elastic hydrogel-based microelectronics for localized low-voltage neuromodulation. *Nat. Biomed. Eng.* **3**, 58–68 (2019).
29. H. Yuk, B. Lu, X. Zhao, Hydrogel bioelectronics. *Chem. Soc. Rev.* **48**, 1642–1667 (2019).
30. B. Mirani, E. Pagan, B. Currie, M. A. Siddiqui, R. Hosseinzadeh, P. Mostafalu, Y. S. Zhang, A. Ghahary, M. Akbari, An advanced multifunctional hydrogel-based dressing for wound monitoring and drug delivery. *Adv. Healthc. Mater.* **6**, 1700718 (2017).
31. M. Omidi, A. Yadegari, L. Tayebi, Wound dressing application of pH-sensitive carbon dots/chitosan hydrogel. *RSC Adv.* **7**, 10638–10649 (2017).
32. J. Bae, J. Park, S. Kim, H. Cho, H. J. Kim, S. Park, D.-S. Shin, Tailored hydrogels for biosensor applications. *J. Ind. Eng. Chem.* **89**, 1–12 (2020).
33. D. Wang, Y. Hu, P. Liu, D. Luo, Bioresponsive DNA hydrogels: Beyond the conventional stimuli responsiveness. *Acc. Chem. Res.* **50**, 733–739 (2017).
34. S. Y. C. Tong, J. S. Davis, E. Eichenberger, T. L. Holland, V. G. Fowler Jr., Staphylococcus aureus infections: Epidemiology, pathophysiology, clinical manifestations, and management. *Clin. Microbiol. Rev.* **28**, 603–661 (2015).
35. E. T. M. Berends, A. R. Horswill, N. M. Haste, M. Monestier, V. Nizet, M. von Köckritz-Blickwede, Nuclease expression by staphylococcus aureus facilitates escape from neutrophil extracellular traps. *J. Innate Immun.* **2**, 576–586 (2010).
36. P. Sharma, N. Garg, A. Sharma, N. Capalash, R. Singh, Nucleases of bacterial pathogens as virulence factors, therapeutic targets and diagnostic markers. *Int. J. Med. Microbiol.* **309**, 151354 (2019).
37. V. Papayannopoulos, Neutrophil extracellular traps in immunity and disease. *Nat. Rev. Immunol.* **18**, 134–147 (2018).
38. H. U. Chung, B. H. Kim, J. Y. Lee, J. Lee, Z. Xie, E. M. Ibler, K. Lee, A. Banks, J. Y. Jeong, J. Kim, C. Ogle, D. Grande, Y. Yu, H. Jang, P. Assem, D. Ryu, J. W. Kwak, M. Namkoong, J. B. Park, Y. Lee, D. H. Kim, A. Ryu, J. Jeong, K. You, B. Ji, Z. Liu, Q. Huo, X. Feng, Y. Deng, Y. Xu, K.-I. Jang, J. Kim, Y. Zhang, R. Ghaffari, C. M. Rand, M. Schau, A. Hamvas, D. E. Weese-Mayer, Y. Huang, S. M. Lee, C. H. Lee, N. R. Shanbhag, A. S. Paller, S. Xu, J. A. Rogers, Binodal, wireless epidermal electronic systems with in-sensor analytics for neonatal intensive care. *Science* **363**, eaau0780 (2019).
39. A. J. Bandodkar, P. Gutruf, J. Choi, K. Lee, Y. Sekine, J. T. Reeder, W. J. Jeang, A. J. Aranyosi, S. P. Lee, J. B. Model, R. Ghaffari, C.-J. Su, J. P. Leshock, T. Ray, A. Verrillo, K. Thomas,

V. Krishnamurthi, S. Han, J. Kim, S. Krishnan, T. Hang, J. A. Rogers, Battery-free, skin-interfaced microfluidic/electronic systems for simultaneous electrochemical, colorimetric, and volumetric analysis of sweat. *Sci. Adv.* **5**, eaav3294 (2019).
40. P. Karacan, H. Cakmak, O. Okay, Swelling behavior of physical and chemical DNA hydrogels. *J. Appl. Polym. Sci.* **128**, 3330–3337 (2013).
41. T. Amiya, T. Tanaka, Phase transitions in crosslinked gels of natural polymers. *Macromolecules* **20**, 1162–1164 (1987).
42. J. Wu, Z. Wu, H. Xu, Q. Wu, C. Liu, B.-R. Yang, X. Gui, X. Xie, K. Tao, Y. Shen, J. Miao, L. K. Norford, An intrinsically stretchable humidity sensor based on anti-drying, self-healing and transparent organohydrogels. *Mater. Horiz.* **6**, 595–603 (2019).
43. C. Gong, D. Liu, Z. Miao, M. Li, A magnetic-balanced inductive link for the simultaneous uplink data and power telemetry. *Sensors* **17**, 1768 (2017).
44. A. K. RamRakhyani, G. Lazzi, On the design of efficient multi-coil telemetry system for biomedical implants. *IEEE Trans. Biomed. Circuits Syst.* **7**, 11–23 (2013).
45. S. S. Ivković, M. Z. Marković, D. Ž. Ivković, N. Cvetanović, LCR circuit: New simple methods for measuring the equivalent series resistance of a capacitor and inductance of a coil. *Eur. J. Phys.* **38**, 055705 (2017).
46. S. E. Gardner, R. A. Frantz, C. L. Saltzman, S. L. Hillis, H. Park, M. Scherubel, Diagnostic validity of three swab techniques for identifying chronic wound infection. *Wound Repair Regen.* **14**, 548–557 (2006).
47. K. K. L. Chong, W. H. Tay, B. Janela, A. M. H. Yong, T. H. Liew, L. Madden, D. Keogh, T. M. S. Barkham, F. Ginhoux, D. L. Becker, K. A. Kline, Enterococcus faecalis modulates immune activation and slows healing during wound infection. *J. Infect. Dis.* **216**, 1644–1654 (2017).
48. C. P. Parlet, M. M. Brown, A. R. Horswill, Commensal staphylococci influence staphylococcus aureus skin colonization and disease. *Trends Microbiol.* **27**, 497–507 (2019).
49. C. Hauser, B. Wuethrich, L. Matter, J. A. Wilhelm, W. Sonnabend, K. Schopfer, *Staphylococcus aureus* skin colonization in atopic dermatitis patients. *Dermatology* **170**, 35–39 (1985).
50. H. Yuk, T. Zhang, G. A. Parada, X. Liu, X. Zhao, Skin-inspired hydrogel–Elastomer hybrids with robust interfaces and functional microstructures. *Nat. Commun.* **7**, 12028 (2016).
51. J. T. Reeder, J. Choi, Y. Xue, P. Gutruf, J. Hanson, M. Liu, T. Ray, A. J. Bandodkar, R. Avila, W. Xia, S. Krishnan, S. Xu, K. Barnes, M. Pahnke, R. Ghaffari, Y. Huang, J. A. Rogers, Waterproof, electronics-enabled, epidermal microfluidic devices for sweat collection, biomarker analysis, and thermography in aquatic settings. *Sci. Adv.* **5**, eaau6356 (2019).
52. M. A. English, L. R. Soenksen, R. V. Gayet, H. de Puig, N. M. Angenent-Mari, A. S. Mao, P. Q. Nguyen, J. J. Collins, Programmable CRISPR-responsive smart materials. *Science* **365**, 780–785 (2019).
53. E. Hidalgo, C. Domínguez, Study of cytotoxicity mechanisms of silver nitrate in human dermal fibroblasts. *Toxicol. Lett.* **98**, 169–179 (1998).
54. Y. Liu, Y. Zhao, B. Sun, C. Chen, Understanding the toxicity of carbon nanotubes. *Acc. Chem. Res.* **46**, 702–713 (2013).
55. A. B. Seabra, A. J. Paula, R. de Lima, O. L. Alves, N. Durán, Nanotoxicity of graphene and graphene oxide. *Chem. Res. Toxicol.* **27**, 159–168 (2014).
56. J. Zhang, L. Mou, X. Jiang, Surface chemistry of gold nanoparticles for health-related applications. *Chem. Sci.* **11**, 923–936 (2020).
57. S. Lin, H. Yuk, T. Zhang, G. A. Parada, H. Koo, C. Yu, X. Zhao, Stretchable hydrogel electronics and devices. *Adv. Mater.* **28**, 4497–4505 (2016).
58. J. Ren, L. Li, C. Chen, X. Chen, Z. Cai, L. Qiu, Y. Wang, X. Zhu, H. Peng, Twisting carbon nanotube fibers for both wire-shaped micro-supercapacitor and micro-battery. *Adv. Mater.* **25**, 1155–1159 (2013).
59. X. Lu, P. Wang, D. Niyato, D. I. Kim, Z. Han, Wireless charging technologies: Fundamentals, standards, and network applications. *IEEE Commun. Surv. Tutor.* **18**, 1413–1452 (2016).
60. Y. Yu, J. Nassar, C. Xu, J. Min, Y. Yang, A. Dai, R. Doshi, A. Huang, Y. Song, R. Gehlhar, A. D. Ames, W. Gao, Biofuel-powered soft electronic skin with multiplexed and wireless sensing for human-machine interfaces. *Sci. Robot.* **5**, eaaz7946 (2020).
61. M. Eriksson, S. K. Kim, S. Sen, A. Graeslund, B. Jernstroem, B. Norden, Location of excimer-forming adducts of (+)-anti-benzo[a]pyrenediol epoxide in DNA. *J. Am. Chem. Soc.* **115**, 1639–1644 (1993).
62. M. Koskinen, K. Plná, Specific DNA adducts induced by some mono-substitued epoxides in vitro and in vivo. *Chem. Biol. Interact.* **129**, 209–229 (2000).
63. R. Milo, R. Phillips, *Cell Biology by the Numbers* (Garland Science, Taylor & Francis Group, 2015).

Acknowledgments: We thank the National University of Singapore Medicine Confocal Microscopy Unit for supporting confocal imaging and Y. X. Guo for facilitating the dielectric measurements. **Funding:** J.S.H. acknowledges support from grants from the National Research Foundation Singapore (NRFF2017-07 and AISG-GC-2019-002), Ministry of Education Singapore (MOE2016-T3-1-004), and Institute for Health Innovation and Technology. D.L.B. acknowledges support from the Agency for Science, Technology and Research (A*STAR) under its Industry Alignment Fund–Pre-Positioning Programme (IAF-PP) grant (H17/01/a0/0C9) as part of the Wound Care Innovation for the Tropics Programme, IAF-PP grant (H17/01/a0/004), and Skin Research Institute of Singapore, Phase 2: SRIS@Novena. H.L. acknowledges support from the Wound Care Innovation for the Tropics Programme, A*STAR IAF-PP grant (H19/01/a0/0GG9), Skin Innovation grant (SIG18005), MOE AcRF Tier 1 grant (R-143-000-B79-114), and Singapore Ministry of Health's National Medical Research Council OF-IRG (MOH-000612-00). W.L. acknowledges support from MOE AcRF Tier 1 grant (R-221-000-093-133). B.C.K.T. acknowledges support from National University of Singapore Startup Grant (NUS-2017-01) and Agency of Science Technology and Research Singapore (A18A1B0045). H. Yao acknowledges Research Scholarship from NUS Materials Science and Engineering. Y.G. acknowledges support from the EMULSION Programme H18/01/A0/017 (IAF-PP, A*STAR). S.M.P.K. acknowledges support from the National Research Foundation Singapore, under its NRF Large Equipment Grants–Grant Addendum 3: Operations of the Singapore Synchrotron Light Source (SSLS). **Author contributions:** Z.X. and J.S.H. conceived and guided the research. Z.X. and S.A. designed and tested the wireless sensor. Z.X., S.L., W.C., V.K., P.S., W.L., and H.L. conducted and contributed to DNAgel bioresponse studies. K.S., G.S.H.C., and B.Y.T. performed and guided patient sample collection and analysis. H. Yang, P.-Y.C., S.P.H., S.M.P.K., M.B.H.B., H. Yao, and B.C.K.T. contributed to DNAgel modification studies. L.E.M., Z.X.O., Y.G., C.T.L., and D.L.B. performed and guided animal studies. Z. Li and Z. Liu supported the characterization of the wireless sensor. Z.X. and J.S.H. wrote the paper with input from all the authors. **Competing interests:** J.S.H., Z.X., S.A., and S.L. are inventors on a pending patent related to this work filed by Intellectual Property Office of Singapore (IPOS), 10202108822V, filed on 12 August 2021. The authors declare no other competing interests. **Data and materials availability:** All data needed to evaluate the conclusions in the paper are present in the paper and/or the Supplementary Materials.

Submitted 27 April 2021
Accepted 1 October 2021
Published 19 November 2021
10.1126/sciadv.abj1617

ScienceAdvances

A wireless and battery-free wound infection sensor based on DNA hydrogel

Ze XiongSippanat AchavananthadithSophie LianLeigh Edward MaddenZi Xin OngWisely ChuaViveka KalidasanZhipeng LiZhu LiuPriti SinghHaitao YangSascha P. HeusslerS. M. P. KalaiselviMark B. H. BreeseHaicheng YaoYuji GaoKavitha SanmugamBenjamin C. K. TeePo-Yen ChenWeiqiang LokeChwee Teck LimGrace Shu Hui ChiangBoon Yeow TanHao LiDavid Laurence BeckerJohn S. Ho

Sci. Adv., 7 (47), eabj1617. • DOI: 10.1126/sciadv.abj1617